metals

MDPI

Review

Analysis of Weak Zones in Friction Stir Welded Magnesium Alloys from the Viewpoint of Local Texture: A Short Review

Dejia Liu *, Yanchuan Tang, Mingxue Shen, Yong Hu and Longzhi Zhao *

School of Materials Science and Engineering, East China Jiaotong University, Nanchang 330013, China; jamestyc@sina.com (Y.T.); shenmingxue@126.com (M.S.); huyong2136@163.com (Y.H.)

* Correspondence: ldj515@126.com (D.L.); zhaolongzhi@163.com (L.Z.); Tel.: +86-791-8704-6718 (D.L.); +86-791-8704-6524 (L.Z.)

Received: 19 October 2018; Accepted: 9 November 2018; Published: 20 November 2018

Abstract: Friction stir welding (FSW) is a promising approach for the joining of magnesium alloys. Although many Mg alloys have been successfully joined by FSW, it is far from industrial applications due to the texture variation and low mechanical properties. This short review deals with the fundamental understanding of weak zones from the viewpoint of texture analysis in FSW Mg alloys, especially for butt welding. Firstly, a brief review of the microstructure and mechanical properties of FSW Mg alloys is presented. Secondly, microstructure and texture evolutions in weak zones are analyzed and discussed based on electron backscatter diffraction data and Schmid factors. Then, how to change the texture and strengthen the weak zones is also presented. Finally, the review concludes with some future challenges and research directions related to the texture in FSW Mg alloys. The purpose of the paper is to provide a basic understanding on the location of weak zones as well as the weak factors related to texture to improve the mechanical properties and promote the industrial applications of FSW Mg alloys.

Keywords: friction stir welding; magnesium alloys; local texture; weak zones; mechanical properties; Schmid factor

1. Introduction

As the lightest structural materials, magnesium and its alloys have excellent specific strength, high specific rigidity, good cast-ability, hot formability, excellent machinability, good electromagnetic interference shielding and recyclability [1,2]. Mg alloys are emerging as important engineering materials, especially in the automotive, rail transit, marine, and aerospace industries [1–3]. Welding is essential for the development of manufactured products. Currently, riveting, fusion welding and hybrid welding are common methods used to join Mg alloys [4]. However, welding defects such as hot cracks, pores, the loss of alloying elements as well as coarse grains are commonly presented in fusion welding of Mg alloys [5]. Most hybrid welding methods are mixing fusion welding and other joining methods [6,7]. Welding defects also exist in these joints. The hybrid welding process is more complicated. Self-piercing riveting (SPR) is another effective method to join Mg alloys [8]. Liu et al. [9] found that equivalent strength of dissimilar joints of AA7075/AZ31 by friction SPR was higher than the yield strength of AZ31 Mg alloy. Durandet et al. [10] found that laser preheating can enhance the dynamic recrystallization (DRX) and prevent cracking, which causes an acceptable strength of the joint of AZ31 alloy prepared by SPR. Haque et al. [11] suggested that assistive technologies help to improve the quality of SPR joints, but some important issues remain to be resolved, such as the corrosion resistance of Mg joints welded by SPR [12]. Therefore, the joining of Mg alloys, a key factor for the industrial application of Mg alloys, is still restricted.

Friction stir welding (FSW) was developed by The Welding Institute (TWI) of the United Kingdom in 1991 [13]. During the welding process, a non-consumable rotating pin is inserted into the faying surface of the plates. Friction heat between the welding tool and the workpiece provides heat to soften the material. The softened material plastically flows around the stirring tool. Finally, the joining process is accomplished with the help of the forging force [14]. As a solid-state joining technique, FSW has significant advantages in welding Mg alloys [15]. Many Mg alloys, such as AZ31, AZ61, AZ91, AM60, ZK60, etc. have been successfully joined by FSW [16–21]. However, it is noted that the studies are mainly carried out in laboratories. It seems to be far from industrial applications, which is mainly related to the microstructure and texture variation in welds of Mg alloys.

Currently, there are several review papers on FSW. For example, Mishra et al. [14] and Ma et al. [22] firstly reviewed the understanding and development of FSW and friction stir processing (FSP). Nandan et al. [23] systematically reviewed the recent advances in FSW, including the process, weldment structure and properties. Çam et al. [15] gave an overview of the welded structural materials beyond Al-alloys for FSW. Fujii et al. [24] reviewed the FSW of steels. Li et al. [25] reviewed the microstructure evolution and mechanical properties of Mg alloys during FSW. Singh et al. [26] comprehensively described the tool geometry, welding parameters, joint configuration, microstructural evolution, residual stresses, mechanical properties and applications of FSW Mg alloys. However, few comprehensive review papers concentrate on the texture in FSW Mg alloys, which has an impact on the mechanical properties and fracture behavior of the joints. To provide an in-depth understanding of the effect of local texture on mechanical properties of FSW Mg alloys, and to improve the mechanical properties of joints, this paper firstly presents a brief review of microstructure and mechanical properties of FSW Mg alloys in Section 2. Secondly, the microstructure and texture evolutions in weak zones are analyzed and discussed based on electron backscatter diffraction (EBSD) data and Schmid factor (SF) values in Section 3. Then, how to change the texture and strengthen the weak zones are shown in Section 4. Finally, future challenges and research directions for texture variation of FSW Mg alloys are presented in Section 5.

2. A Brief Review of Microstructure and Mechanical Properties of FSW Mg Alloys

During FSW, intense plastic deformation occurs in the weld zone (WZ). Dynamic recrystallization causes dramatic changes of microstructure in the WZ and seriously affects the mechanical properties of joints. Therefore, it is meaningful to explore the relationships between microstructure and mechanical properties of FSW Mg alloys. Indeed, there are many published papers on the subject [27–30]. The grains in WZ can be significantly refined during FSW, especially for cast Mg alloys [22,31–36]. The average grain size in WZ for AZ (Mg-Al-Zn) and AM (Mg-Al-Mn) series of Mg alloys is usually about 8–12 μm [1,37–39]. For some special Mg alloys, such as ZK60 alloy, due to the presence of Zr-rich precipitates, grain size can be reduced to 3–5 μm in WZ. In addition, the grain size can be further reduced by using some special methods. For example, nano-grains are obtained in FSW AZ31 alloy by liquid nitrogen cooling [34]. Refined grains in WZ would have beneficial effects on the mechanical properties of FSW Mg alloys.

Precipitation is another factor affecting the mechanical properties of FSW Mg alloys. Precipitates in Mg alloys are commonly broken up during FSW [40–42]. In addition, precipitates would be diffuse and uniformly distributed in WZ. For example, precipitates in the cast and aged ZK60 alloy are segregated along grain boundaries in base metal (BM) and are broken up and changed into a uniform distribution after FSW [42,43]. Therefore, regardless of grain size or precipitates, the mechanical properties of Mg alloys would be enhanced by FSW. Statistical results about alloy types, thickness, welding parameters and tensile properties of FSW Mg alloys are presented in Table 1. It should be stated that the data are mainly about friction stir butt welding Mg alloys. It is found that the joints usually show a lower tensile strength than that of the BMs, especially for wrought Mg alloys [27,37–39,43–57]. Table 1 presents that yield strength (YS) of the joints is only 40–80% of BM. The ultimate tensile strength (UTS) of joints is much lower than that of the BMs. Joint efficiency is calculated as the UTS of joint divided by that of the

BM. Table 1 shows the joint efficiency of FSW Mg alloys usually in the range of 50–95%. There is no doubt that defects such as voids, lack of penetration, etc. have an impact on the mechanical properties of the welds. However, more scholars attributed the phenomenon to other factors related to texture. The low mechanical properties may be the main reason for limiting industrial applications of FSW Mg alloys.

For the hexagonal close-packed Mg, due to the asymmetry of crystal structure, texture has an impact on the plastic deformation and strength of materials. It is well known that the YS is mainly determined by the critical resolved shear stress (CRSS) and SF values, while the UTS is largely affected by work hardening as well as the fracture behavior in weak zones. In most cases, FSW/FSP Mg alloys fractured near the interface of WZ and transition zone (TZ) on advancing side (AS) [27,37,61,82–84]. Therefore, the WZ/TZ interface is speculated to be a weak zone [29,61]. It should be noted that weak factors in these weak zones of FSW Mg alloys may significantly differ from such defects as voids, lack of penetration, channels, etc. However, it can accelerate fracture and reduce the mechanical properties of FSW Mg alloys. In fact, there are several weak zones related to the texture in FSW Mg alloys [82,84,85], including the WZ/TZ interface, stir zone (SZ)-side, triple junction region and SZ-center. The rough locations of these weak zones are provided in Figure 1. Different colors in Figure 1 represent the different locations of weak zones. Exploring the location of weak zones and revealing the weak factors have significantly positive effects on the improvement of the mechanical properties of FSW Mg alloys. Therefore, in this short review, microstructure, local texture and plastic deformations in weak zones are analyzed and discussed based on EBSD data. Finally, how to change the texture and strengthen the weak zones is provided in Section 4.

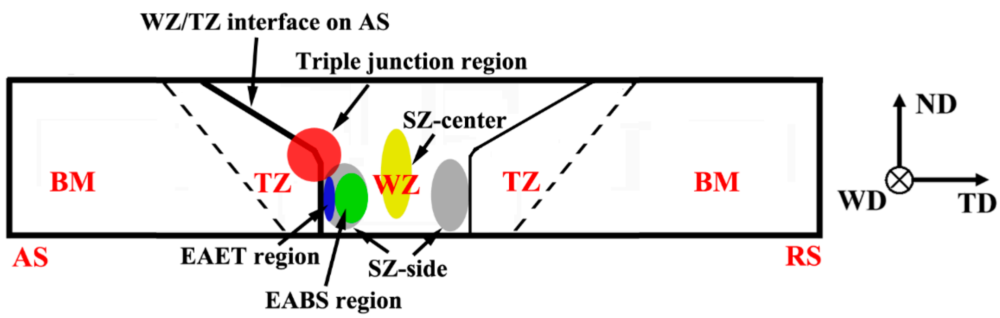

Figure 1. Schematic diagram of weak zones in FSW Mg alloys from the viewpoint of local texture.

Table 1. Summary of tensile properties of FSW Mg-alloys.

Materials	Thickness, mm	Rotation Speed, rpm	Traverse Speed, mm/min	YS of BM, MPa	UTS of BM, MPa	YS of Joint, MPa	UTS of Joint, MPa	Joint Efficiency	Elongation of Joint	Refs.
AZ31B-H24	2	2000	300–1800	-	~282	150–180	200–220	70.9–78%	1.6–2.4%	[58]
	2	2000	600	200	280	~155	200	71.4%	4%	[47]
	3.175	1500–2000	78–204	227.6	307.7	95–115.3	200–225.6	66.4–75%	2.8–22%	[59]
	4	1600	87–507	222.7	293	125–135	180–225.6	61.4–77%	3–4%	[60]
	4	1200–1600	100–200	281	321	100–114	185–211	59.2–65.7%	1.6–2.8%	[61]
	4	2000	100	220	290	93	230	80%	10.24%	[62]
	4	1250–2500	87–507	222.7	293	-	240	85%	5.85%	[60]
	4.95	1000	120–240	208	306	96–115	178–208	58.2–68%	2.5%	[63]
	4.95	500–1000	60–240	208	309	~100–130	170–201	55–65%	2.5%	[64]
AZ31	4	960–2880	10–20	97	210	80–150	180–200	84.9–94%	0.25–1.19%	[65]
	4	375–2250	20–375	-	~274	-	190–255	69.3–93%	-	[66]
	6	1600	600	70	295	86	276	93.6%	4.5%	[27]
	5	900–1400	40	171	215	117–148	139–188	64.6–87.5%	5.1–7.3%	[49]
	6.3	800	100	153	249.5	104–105	203.4–215.6	81.5–86.4%	5.3–10.9%	[37]
	6.3	3500	100	153	249.5	92–117	215.6–237.5	86.4–95.2%	5.3–10.9%	[29]
	6.4	800–3000	100	-	275	115–126	192–233	69.8–84.7%	-	[67]
AZ31B	0.5	2000–4000	80–120	207	286	135–194	185–260	72.3–90.1%	0.8–2.49%	[51]
	3	630–1000	63–100	-	274	-	162–253	59.1–92.3%	1.8–4.7%	[68]
	4	200–300	500	70	231	75	225–232.5	97.4–101%	18%	[57]
	4	600–1100	300–500	70	~230	~75	224	~97%	18.3%	[69]
	4	600–2000	12–2000	300	305	-	~210–293	68.8–96.1%	9–15.1%	[1]
	5	1200–1400	30–50	-	292.9	-	231.2–257.4	78.9–87.9%	3.7–6.7%	[70]
	5	900–1400	25–75	171	215	117–148	139–188	64.7–87.4%	5.1–7.3%	[55]
	6	1600	40.2	171	215	84–138	108–208	50–97%	4.0–7.3%	[71,72]
	6.5	600	58.2	-	230	-	200	87%	12–41%	[73]
AZ61	4	1400	25	219	270	175	220	81.5%	7.2%	[50]
	4.8	400–1500	200–500	202.3	289	169.1–180.7	229.3–294.3	79.3–101.8%	2.4–13.4%	[54]
	6.3	1220	90	~170	~300	~110	~282	94%	~17%	[74]
AZ61A	6	1200	90	217	271	-	117–223	43.2–82.3%	-	[75]
	6	800–1600	30–150	217	271	-	126–224	46.5–82.7%	3.4–7.2%	[16]
AZ61A-F	4	700	160	-	302	123	210	69.5%	3.4–10.24%	[62]
AM60	2	500–1000	120	135	210	-	192–195	91.4–92.8%	5%	[76]
ZM21	5–25	450–600	20–45	120	227	106–102	173–198	76.2–87.2%	5%	[77]
	2	850–1150	22–38	185	283	130–145	170–188	60.1–66.4%	3.97–6.81%	[52]
Mg-6Al-0.4Mn-2Ca	3	20–600	10–100	105	270	54–96	168–265	62.2–98.1%	7%	[48]
Mg–6Sn–2Zn	8	1200	60–120	70.4	186	71.2–77	165–184	88.7–98.9%	26.8–37.2%	[53]
ZK60	6	800	100	~165	~290	~125	~250	87%	18.7%	[78]
ZK60(after HT)	6	800	100	~165	~290	~150	272.9	94%	20%	[78]
Mg-Zn-Y-Zr	6	800	100	~120	~275	~110	~261	95%	~23%	[79]
AZ31-AZ91	3	1400–1800	25–100	175	197	163–181	168–198	85.3–101%	5.1–8.5%	[56]
AZ91	5	900	63	-	128	-	194	151.5%	18%	[30]
AZ91C-F	4	500	50	114	244	109	166	68%	3.4%	[62]
AZ91D	2	800–1800	90–750	-	-	-	-	-	-	[80]
AZ91D	4	115–377 rad/s	32–187	-	110	-	142–162	145%	-	[81]

"-" indicates the data are not provided in the reference.

3. Microstructure and Texture in Weak Zones

3.1. Interface of WZ/TZ

As mentioned above, DRX causes grain refinement in Mg alloys after FSW (in most cases) [31,34,86], which leads to large differences in grain size between the WZ and TZ. Therefore, the interfaces of WZ/TZ are clearly observed by macroscopic observation, especially for cast Mg alloys [61,87,88]. The clear interface indicates a dramatic variation of microstructure on two sides of the interface, implying that the interface of WZ/TZ would be a weak zone of FSW Mg alloys. For some special alloys, little difference in grain size is observed between the WZ and TZ. The interfaces of WZ/TZ are less clear. However, significantly different characteristics of the interface are observed in AS and retreating side (RS) [37,64,87,89–91]. Figure 2 shows that the interface of WZ/TZ is clearly observed in AS. However, that in RS is less clear. Steuwer et al. [89] deeply studied the different formations of WZ/TZ interfaces in AS and RS. Material flows forwards in AS experiencing a shear stress, which leads to a narrow deformation zone adjacent to the WZ/TZ interface. Then, a clear interface is presented in AS [89]. However, for the RS, material flows are trapped and extruded during the transferring from AS to RS, which leads to a wider, less severe strain gradient in RS [89,91]. Then, a less clear interface of WZ/TZ is formed in RS (see Figure 2c).

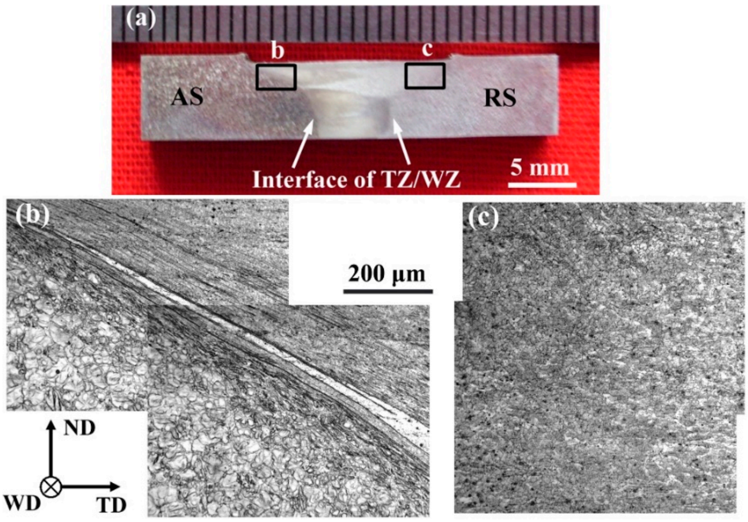

Figure 2. Interfaces between the TZ and WZ of FSW Mg alloys: (**a**) macro photo; (**b**) the interface in AS; and (**c**) the interface in RS [83].

In addition to the large variation of grain size between WZ and TZ, different textures are observed on two sides of the WZ/TZ interface. EBSD orientation maps of the SZ/TZ interfaces of FSW AZ31 Mg alloy are shown in Figure 3 and the inverse pole figure (IPF) is color-coded according to the transverse direction (TD) [92]. It is noted that the difference in grain size between the SZ and TZ is not evident. However, clear interfaces of SZ/TZ with different colors are observed in both the AS and RS (see Figure 3), indicating different grain orientations in the TZ and SZ. Woo et al. [73] reported that significant texture variations between the TZ and SZ can cause inhomogeneous deformation and lead to the fracture near the SZ/TZ interface. There is no doubt that large texture variations at the SZ/TZ interface can accelerate fracture and reduce the mechanical properties of FSW Mg alloys. Therefore, the interface of WZ/TZ, especially for that in AS, is a significant weak zone for FSW Mg alloys. Indeed, there are many FSW Mg alloys fractured at or near the interface of WZ/TZ in AS during transverse tensile tests [1,27], confirming that the interface of WZ/TZ in AS is a significant weak zone.

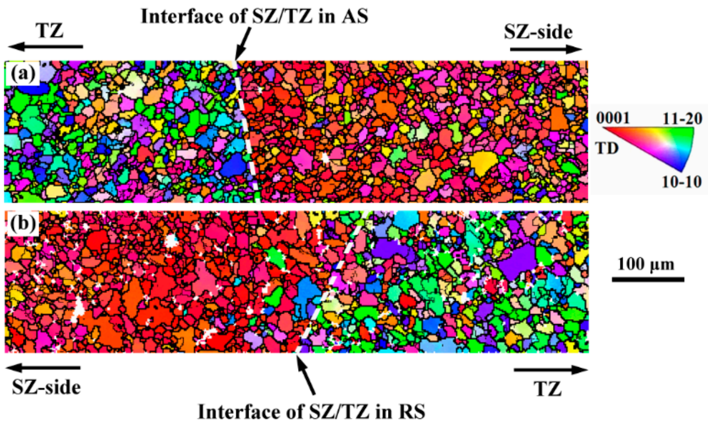

Figure 3. EBSD orientation maps of the SZ/TZ interfaces in FSW AZ31 alloy: (**a**) AS; and (**b**) RS [92].

3.2. SZ-Side

In addition to grain refinement, a strong texture is formed in FSW Mg alloys [28,31,32,73,93,94]. Textures in typical regions of FSW AZ31 plate are presented in Figure 4 [82]. The corresponding positions are shown in Figure 4a. Significantly different textures are found in various regions (see Figure 4b). BM shows a typical characteristic of hot-rolled Mg-alloy plate with the c-axis parallel to the normal direction (ND). SZ-center (position of a_1 in Figure 4a) shows the c-axis of most grains perpendicular to the TD, while SZ-side (position of a_2) presents a texture with the c-axis nearly parallel to the TD. Basal slip and extension twinning are most easily activated at room temperature for Mg alloys due to the low CRSS [95,96]. The activation of basal slip and extension twinning can be predicted by SF values based on EBSD data. Figure 4c shows that SZ-side has the highest SF value (~0.4), while SZ-center presents the lowest SF value (~0.14). The results indicate that basal slip is easily activated in SZ-side and hardly activated in SZ-center. Therefore, SZ-side would be a weak zone for FSW Mg alloys, compared with the SZ-center as well as the BM.

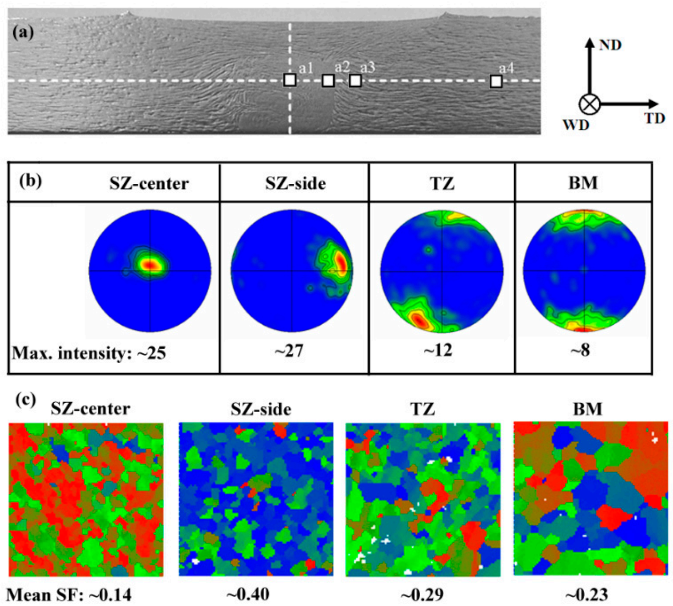

Figure 4. EBSD orientation maps of various regions in FSW AZ31 alloy: (**a**) measurement positions; (**b**) {0001} pole figures; and (**c**) SF maps of basal slip in various regions during the transverse tensile tests [84].

To deeply understand the weak factors from the viewpoint of local texture in SZ-side, SF maps of extension twinning and basal slip in SZ-side of FSW AZ31 alloy are studied based on EBSD data. Figure 5 shows that a narrow region in SZ-side close to the SZ/TZ interface presents the highest SF value for extension twinning (the blue zone in Figure 5a). A relatively wide region, which is slightly away from the SZ/TZ interface, shows the highest SF value for basal slip (the blue zone in Figure 5b). The results indicate that dominant deformation mechanisms in SZ-side are changed from extension twinning to basal slip as the region moving away from the SZ/TZ interface [84].

Based on the SF values, SZ-side can be divided into two micro-regions. One is the Easy to Activate Extension Twinning region (EAET region), which is close to the SZ/TZ interface. The other is slightly away from the SZ/TZ interface, named as the Easy to Activate Basal Slip region (EABS region). {0001} pole figures of various micro-regions are presented in Figure 5c, indicating that the c-axis is inclined about 10° towards TD in EAET region, while it is inclined about 40° towards TD in EABS region. It confirms that it is easy to activate extension twinning in the EAET region, while it is easy to activate basal slip in the EABS region during transverse tensile tests [84]. In addition, it is found that EAET region is very narrow, only about 100 μm wide along the TD (see Figure 5). The activation of different deformations in such a narrow zone of SZ-side may cause plastic deformation incompatibility and initiate fracture. The results fully confirm that SZ-side is a weak zone of FSW Mg alloys.

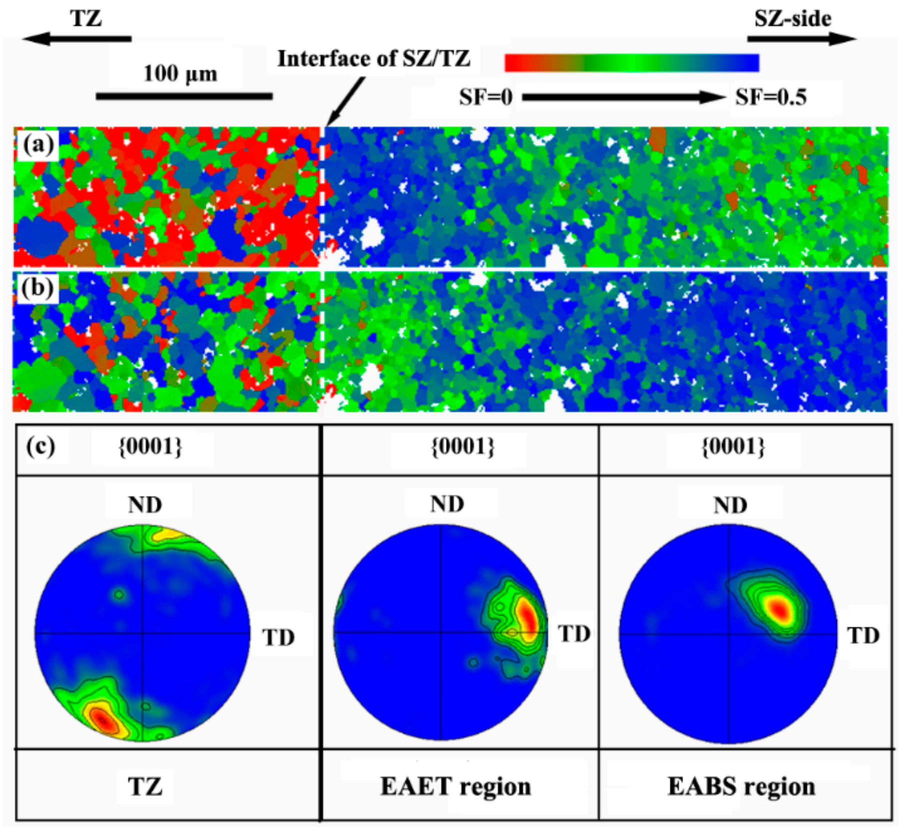

Figure 5. SF maps at the SZ/TZ interface of FSW AZ31 alloy: SF maps for extension twinning (**a**) and basal slip (**b**); and {0001} pole figures in micro-regions near the SZ/TZ interface [84] (**c**).

3.3. Triple Junction Region

A special region is presented adjacent to the WZ/TZ interface and near the transfer region of the crown zone (CZ) and SZ in AS. Because it is near the junction region among the TZ, CZ and SZ, it was named as triple junction region [85]. In fact, the triple junction region widely exists in FSW Mg alloys. However, it may be hardly observed in optical micrographs, because the variation of grain size in triple junction region is not evident. In addition, triple junction region can be observed in AS, but is hardly identified in RS. EBSD maps of the triple junction region of FSW AZ31 alloy are provided in Figure 6. It is confirmed that the variation of grain size in the region is not obvious. However, clear interfaces with different colors are observed in the orientation map, indicating different textures presented in this region [85].

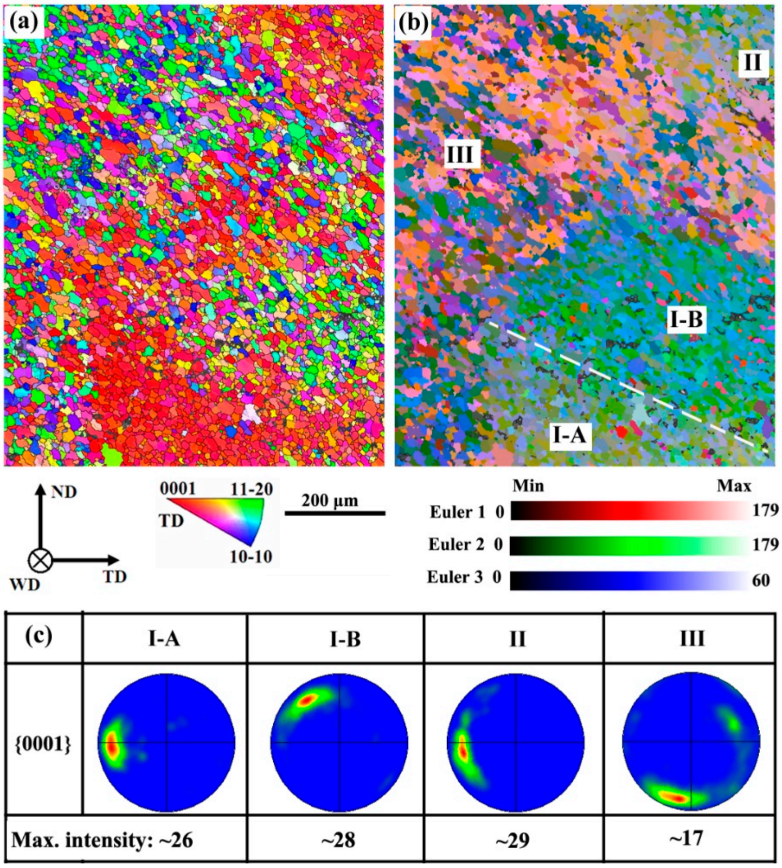

Figure 6. EBSD orientation maps of triple junction region in FSW AZ31 alloy: (**a**) IPF map; (**b**) Euler angle map; and (**c**) texture distributions [85].

Based on the texture distributions, the triple junction region may be divided into four parts: Regions I-A, I-B, II and III (see Figure 6b). Figure 6c shows that the c-axis is inclined about 19° towards TD in Region I-A, while it is inclined about ~56° towards TD in Region I-B. The angles between the c-axis and TD in Regions II and III are ~22° and ~78°, respectively. It is noted that the c-axis of grains in Region I-B has rotated toward ND compared with Region I-A. Therefore, it is speculated that the formation of triple junction region has a close relationship with screw threads of stir tool [83]. The screw threads extrude the materials in Region I-B with a vertical stress during FSW, which causes the c-axis of grains in Region I-B rotated toward the ND. However, the detailed formation mechanism of triple junction region is still unknown.

To explore the plastic deformation mechanisms in the triple junction region, SF values of basal slip and extension twinning in the region are studied. Figure 7 shows that all micro-regions in triple junction region have a high SF value of basal slip (>0.3). It means that basal slip is easily activated in the triple junction region. Moreover, large differences in SF values of extension twinning are observed in the region. The highest SF value of extension twinning is ~0.37 in Region I-A, while the lowest one is 0.11 in Region III. The results indicate that the competition of basal slip and extension twinning in triple junction region is very complex. An incompatible deformation easily occurs in the triple junction region. It was confirmed by a sharp corner appearing close to the triple junction region for the tensile and compressive samples interrupted at 5% strain [97]. Moreover, the authors recently studied different fracture behaviors of FSW AZ31 Mg alloy during Surface and Base bending tests and found that triple junction region has a significant effect on fracture behavior as it is subjected to tensile state, and the effect is much smaller in compression state [98].

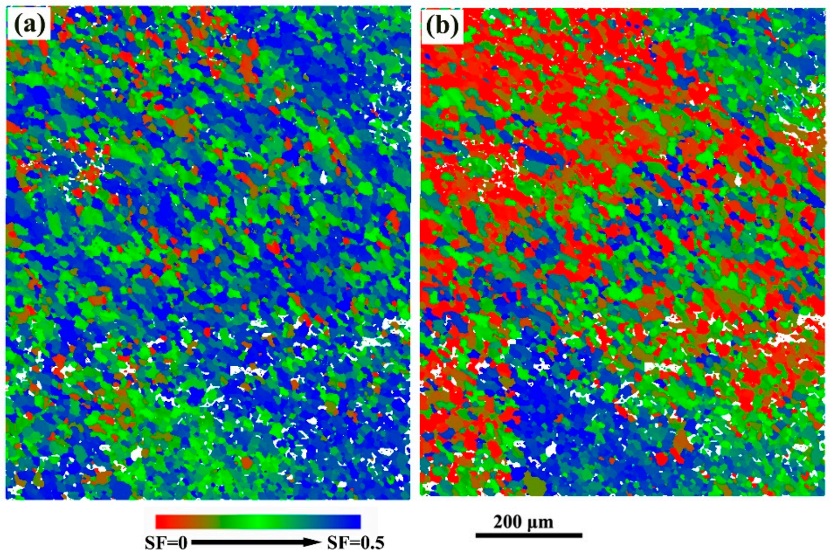

Figure 7. SF maps of triple junction region in FSW AZ31 alloy during the transverse tensile tests: (**a**) SF map for basal slip; and (**b**) SF map for extension twinning.

Triple junction region is also observed at the dissimilar joint of ZK60/AZ31 by FSW [83]. In addition to the texture variation, grain size shows large differences in various micro-regions of the triple junction region [83]. Owing to the presence of triple junction region in AS, the joint is fractured close to ZK60 alloy, the "hard" material side in AS, during the transverse tensile tests. Moreover, a sharp corner is observed in the fracture line of the fractured sample of ZK60/AZ31 joint [83]. The location of sharp corner is near close to the triple junction region. The results confirmed that triple junction region has an impact on the fracture behaviors of FSW Mg alloys, which is a significant weak zone for FSW Mg alloys.

3.4. SZ-Center

The fracture of FSW Mg alloys usually starts at the SZ/TZ interface, and it is propagated toward SZ-center with an inclined angle of ~45° [29,37,78]. Therefore, SZ-center may be another weak zone of FSW Mg alloys. Yang et al. [29] studied the activation of twinning in SZ-center during the transverse tensile tests. They found that twinning is hardly activated in SZ-center as the tensile stress was lower than 75% UTS. However, many compression twins and double twins are detected in SZ-center by EBSD as the tensile stress reached 95% UTS.

In general, compression twinning and double twinning are hardly activated at room temperature due to the high CRSS. However, it may occur in the later stage of deformation due to the high stress. Compression twinning can be activated as the grains are in compression along the c-axis, with an average CRSS value of 112 MPa [96,99]. As uniaxial tensile tests were carried out on tensile samples, there is a compression along the thickness and width directions. The grains in SZ-center exactly present the c-axis nearly paralleling to the thickness direction (i.e., the WD, see Figure 4b). Therefore, there are opportunities to activate compression twinning and double twinning in SZ-center during the transverse tensile tests. The formation of compression twins and double twins may produce a highly localized strain field and induce strain incompatibility and the failure at the twin interfaces [29]. Therefore, SZ-center may be another weak zone of FSW Mg alloys.

Nevertheless, the authors believe that several weak zones related to texture exist in FSW Mg alloys, including the WZ/TZ interface, SZ-side, triple junction region and SZ-center. The approximate locations of weak zones are presented in Figure 1. The weak zones related to texture have an impact on the mechanical properties and fracture behavior of FSW Mg alloys.

4. How to Modify the Local Texture and Strengthen the Weak Zones in FSW Mg Alloys

Researchers tried to modify welding parameters and refine the grains to improve the mechanical properties of FSW Mg alloys [29,37,75,88]. However, Wang et al. [32] found that the texture of Mg alloys can significantly reduce the effect of grain size on the strength of the welds. The main factor affecting the mechanical properties of FSW Mg alloys is not grain size but the local texture in WZ [32]. Lee et al. [100] found that for FSW AZ61 sample, a subsequent compression along the ND can change the texture by inducing deformation twins. The YS can significantly be raised from 140 to 260 MPa. However, it should be stated that the tensile specimen is a pocket one and sampling only from SZ-center. Many weak zones, such as the SZ/TZ interface, SZ-side and triple junction region, are excluded in the test specimen. Therefore, the results cannot represent the entire mechanical properties of the joint after subsequent compression.

To modify the texture and strengthen the weak zones in FSW Mg alloys, subsequent rolling and tensile along the TD were employed in FSW AZ31 alloy [27,101]. Microstructure evolution and twinning behaviors at the SZ/TZ interface (a weak zone) after subsequent deformations are evaluated by EBSD. Figure 8a shows that many extension twins are formed in SZ-side after post-rolling along the TD [101]. The formed twins in SZ-side present a low SF value, especially for extension twinning (see Figure 8b,c). The results confirm that subsequent rolling can change the grains from soft orientations into hard orientations. In addition, SF value of basal slip in SZ-side is always higher than that of extension twinning after post-rolling. It means that the EAET region disappears in SZ-side after post-rolling. The dominant deformation mechanism in SZ-side is basal slip and not changed after post-rolling (see Figure 8d).

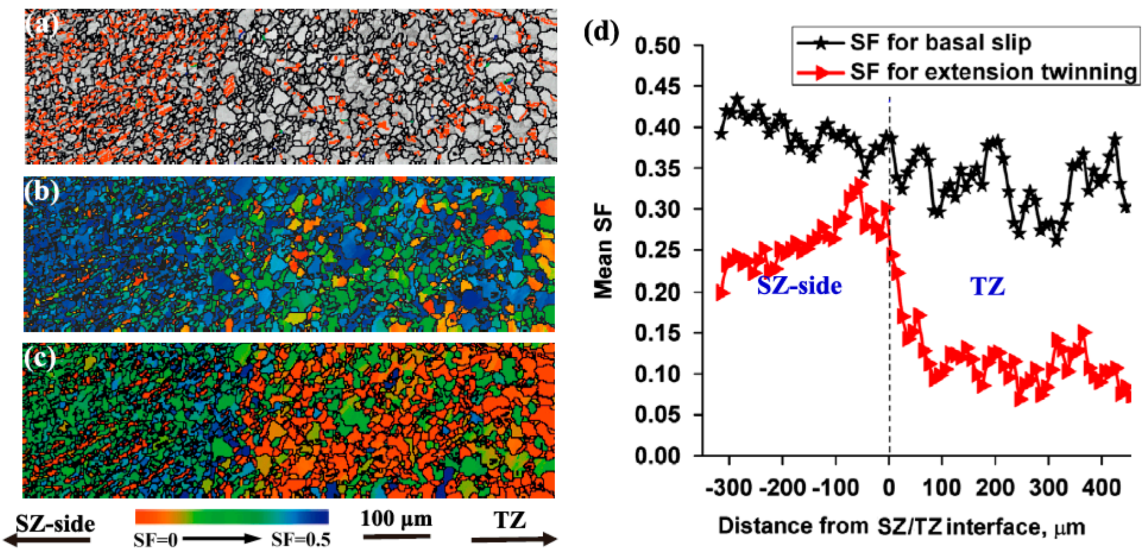

Figure 8. EBSD orientation maps of the SZ/TZ interface in FSW AZ31 alloy with a subsequent rolling strain of 2.5%: (**a**) band contrast map with extension twin boundaries indicated by red lines; SF map for basal slip (**b**) and extension twinning (**c**); and (**d**) variation of SF values as a function of the distance from the SZ/TZ interface [101].

During the subsequent rolling process, fine-grain strengthening and texture strengthening enhance the weak zones in FSW AZ31 alloy. It reduces the inhomogeneous deformation between SZ-center and SZ-side and improves the mechanical properties of the joints. It is reported that the YS is raised from ~87 MPa in the as-welded state to ~171 MPa in the specimens with a rolling strain of ~7%. In addition, subsequent rolling cause the fracture position of FSW Mg alloys changed from SZ-side to

BM [27,101]. Therefore, subsequent deformation along specific directions can significantly enhance the weak zones and improve the mechanical properties of FSW Mg alloys by inducing deformation twins. Moreover, some relationships between welding parameters and texture distributions are found in FSW Mg alloys [102,103]. However, it is difficult to control the texture in WZ by changing the welding parameters so far. Therefore, how to modify the textures in weak zones through a simple and quick method needs further systematic research.

5. Conclusions and Further Works

In this paper, weak zones in FSW Mg alloys and the weak factors from the viewpoint of texture are reviewed. Current situation and some critical scientific problems in the research field are summarized as follows:

(1) Various textures in WZ cause different plastic deformations and several weak zones related to the texture form in FSW Mg alloys. Weak factors in these weak zones significantly differ from such defects as voids, lack of penetration, channels, etc. However, they can accelerate fracture and reduce the mechanical properties of FSW Mg alloys.

(2) The WZ/TZ interface is a weak zone of FSW Mg alloys. Drastic changes of microstructure and texture exist near the WZ/TZ interface, especially for that in AS, which can accelerate fracture and reduce the mechanical properties of the joints. Thus, how to reduce the changes of microstructure and texture in the WZ/TZ interfaces would be an interesting research direction.

(3) SZ-side has large SF values of basal slip and extension twinning during the transverse tensile tests. Dominant deformation mechanisms in SZ-side are transferred from extension twinning to basal slip with greater distance from the SZ/TZ interface. SZ-side can be divided into EAET region and EABS region. FSW Mg alloys could fracture in SZ-side on AS. However, due to the narrow EAET region, the fracture actually occurrs in EAET region or EABS region is still unknown. It is meaningful to confirm whether fracture is initiated in EAET region or EABS region.

(4) Significant differences of microstructure and texture are presented in triple junction region. The complex competition of basal slip and extension twinning results in incompatible deformations in the triple junction region, which has a significant promoting effect on the fracture of FSW Mg alloys. However, the detailed formation of triple junction region is still unclear. How to control the formation of triple junction region needs to be studied.

(5) Subsequent deformation along specific directions can significantly enhance weak zones related to the texture and improve the mechanical properties of FSW Mg alloys by inducing deformation twins. There are some relationships between welding parameters and texture distributions of FSW Mg alloys. However, it is difficult to control the texture in WZ by changing the welding parameters. Therefore, how to modify the textures in weak zones through a simple and quick method needs further systematic research.

Author Contributions: Conceptualization and writing—original draft preparation, D.L.; Software, Y.T.; Formal analysis, M.S.; Supervision, Y.H.; and Funding acquisition, L.Z.

Funding: This research was funded by National Natural Science Foundation of China (grant numbers 51805171, 51865011, and 51761012] and Natural Science Foundation in Jiangxi Province (grant number 20181BAB216021).

Acknowledgments: The authors are thankful to Renlong Xin, College of Materials Science and Engineering, Chongqing University, China for his valuable discussion and guidance.

Conflicts of Interest: The authors declare no conflict of interest.

References

1. Fu, R.D.; Ji, H.S.; Li, Y.J.; Liu, L. Effect of weld conditions on microstructures and mechanical properties of friction stir welded joints on AZ31B magnesium alloys. *Sci. Technol. Weld. Join.* **2012**, *17*, 174–179. [CrossRef]

2. Yuan, W.; Panigrahi, S.K.; Su, J.Q.; Mishra, R.S. Influence of grain size and texture on Hall–Petch relationship for a magnesium alloy. *Scr. Mater.* **2011**, *65*, 994–997. [CrossRef]
3. Liu, Z.; Ji, S.; Meng, X. Joining of magnesium and aluminum alloys via ultrasonic assisted friction stir welding at low temperature. *Int. J. Adv. Manuf. Technol.* **2018**, *97*, 4127–4136. [CrossRef]
4. Quan, Y.; Chen, Z.; Gong, X.; Yu, Z. CO_2 laser beam welding of dissimilar magnesium-based alloys. *Mater. Sci. Eng. A* **2008**, *496*, 45–51. [CrossRef]
5. Rajakumar, S.; Balasubramanian, V.; Razalrose, A. Friction stir and pulsed current gas metal arc welding of AZ61A magnesium alloy: A comparative study. *Mater. Des.* **2013**, *49*, 267–278. [CrossRef]
6. Meng, Y.; Gao, M.; Zeng, X. Quantitative analysis of synergic effects during laser-arc hybrid welding of AZ31 magnesium alloy. *Opt. Lasers Eng.* **2018**, *111*, 183–192. [CrossRef]
7. Hou, Z.-L.; Liu, L.-M.; Lv, X.-Z.; Qiao, J.; Wang, H.-Y. Numerical simulation for pulsed laser–gas tungsten arc hybrid welding of magnesium alloy. *J. Iron Steel Res. Int.* **2018**, *25*, 995–1002. [CrossRef]
8. Li, D.; Chrysanthou, A.; Patel, I.; Williams, G. Self-piercing riveting—A review. *Int. J. Adv. Manuf. Technol.* **2017**, *92*, 1777–1824. [CrossRef]
9. Liu, X.; Lim, Y.C.; Li, Y.; Tang, W.; Ma, Y.; Feng, Z.; Ni, J. Effects of process parameters on friction self-piercing riveting of dissimilar materials. *J. Mater. Process. Technol.* **2016**, *237*, 19–30. [CrossRef]
10. Durandet, Y.; Deam, R.; Beer, A.; Song, W.; Blacket, S. Laser assisted self-pierce riveting of AZ31 magnesium alloy strips. *Mater. Des.* **2010**, *31*, 13–16. [CrossRef]
11. Haque, R. Quality of self-piercing riveting (SPR) joints from cross-sectional perspective: A review. *Arch. Civ. Mech. Eng.* **2018**, *18*, 83–93. [CrossRef]
12. Upadhyay, V.; Qi, X.; Wilson, N.; Battocchi, D.; Bierwagen, G.; Forsmark, J.; McCune, R. Electrochemical characterization of coated self-piercing rivets for magnesium applications. *SAE Int. J. Mater. Manuf.* **2016**, *9*, 187–199. [CrossRef]
13. Thomas, W.M.; Nicholas, E.D.; Needham, J.C.; Murch, M.G.; Templesmith, P.; Dawes, C.J. Friction Stir Butt Welding. Patent Application No. 9125978.8, 6 December 1991.
14. Mishra, R.S.; Ma, Z.Y. Friction stir welding and processing. *Mater. Sci. Eng. R Rep.* **2005**, *50*, 1–78. [CrossRef]
15. Çam, G. Friction stir welded structural materials: Beyond Al-alloys. *Int. Mater. Rev.* **2011**, *56*, 1–48. [CrossRef]
16. Rajakumar, S.; Razalrose, A.; Balasubramanian, V. Friction stir welding of AZ61A magnesium alloy. *Int. J. Adv. Manuf. Technol.* **2013**, *68*, 277–292. [CrossRef]
17. Albakri, A.N.; Mansoor, B.; Nassar, H.; Khraisheh, M.K. Thermo-mechanical and metallurgical aspects in friction stir processing of AZ31 Mg alloy—A numerical and experimental investigation. *J. Mater. Process. Technol.* **2013**, *213*, 279–290. [CrossRef]
18. Dhanapal, A.; Rajendra Boopathy, S.; Balasubramanian, V. Influence of pH value, chloride ion concentration and immersion time on corrosion rate of friction stir welded AZ61A magnesium alloy weldments. *J. Alloys Compd.* **2012**, *523*, 49–60. [CrossRef]
19. Mironov, S.; Onuma, T.; Sato, Y.S.; Kokawa, H. Microstructure evolution during friction-stir welding of AZ31 magnesium alloy. *Acta Mater.* **2015**, *100*, 301–312. [CrossRef]
20. Richmire, S.; Hall, K.; Haghshenas, M. Design of experiment study on hardness variations in friction stir welding of AM60 Mg alloy. *J. Magnes. Alloy.* **2018**, *6*, 215–228. [CrossRef]
21. Mishra, A.; Gupta, A.D.; Sharma, A.K.; Nidigonda, G. Mechanical and microstructure properties analysis of friction stir welded similar and dissimilar Mg alloy joints. *Int. J. Curr. Eng. Technol.* **2018**, *8*. [CrossRef]
22. Ma, Z.Y. Friction stir processing technology: A review. *Metall. Mater. Trans. A* **2008**, *39*, 642–658. [CrossRef]
23. Nandan, R.; Debroy, T.; Bhadeshia, H. Recent advances in friction-stir welding—Process, weldment structure and properties. *Prog. Mater. Sci.* **2008**, *53*, 980–1023. [CrossRef]
24. Fujii, H. Friction stir welding of steels. *Weld. Int.* **2011**, *25*, 260–273. [CrossRef]
25. Li, Y.J.; Qin, F.M.; Liu, C.R.; Wu, Z.S. A review: Effect of friction stir welding on microstructure and mechanical properties of magnesium alloys. *Metals* **2017**, *7*, 524. [CrossRef]
26. Singh, K.; Singh, G.; Singh, H. Review on friction stir welding of magnesium alloys. *J. Magnes. Alloy.* **2018**. [CrossRef]
27. Xin, R.; Sun, L.; Liu, D.; Zhou, Z.; Liu, Q. Effect of subsequent tension and annealing on microstructure evolution and strength enhancement of friction stir welded Mg alloys. *Mater. Sci. Eng. A* **2014**, *602*, 1–10. [CrossRef]

28. Yuan, W.; Mishra, R.S. Grain size and texture effects on deformation behavior of AZ31 magnesium alloy. *Mater. Sci. Eng. A* **2012**, *558*, 716–724. [CrossRef]
29. Yang, J.; Wang, D.; Xiao, B.L.; Ni, D.R.; Ma, Z.Y. Effects of rotation rates on microstructure, mechanical properties, and fracture behavior of friction stir-welded (FSW) AZ31 magnesium alloy. *Metall. Mater. Trans. A* **2012**, *44*, 517–530. [CrossRef]
30. Asadi, P.; Givi, M.K.B.; Parvin, N.; Araei, A.; Taherishargh, M.; Tutunchilar, S. On the role of cooling and tool rotational direction on microstructure and mechanical properties of friction stir processed AZ91. *Int. J. Adv. Manuf. Technol.* **2012**, *63*, 987–997. [CrossRef]
31. Yuan, W.; Mishra, R.S.; Carlson, B.; Mishra, R.K.; Verma, R.; Kubic, R. Effect of texture on the mechanical behavior of ultrafine grained magnesium alloy. *Scr. Mater.* **2011**, *64*, 580–583. [CrossRef]
32. Wang, Y.N.; Chang, C.I.; Lee, C.J.; Lin, H.K.; Huang, J.C. Texture and weak grain size dependence in friction stir processed Mg–Al–Zn alloy. *Scr. Mater.* **2006**, *55*, 637–640. [CrossRef]
33. Feng, A.H.; Ma, Z.Y. Enhanced mechanical properties of Mg–Al–Zn cast alloy via friction stir processing. *Scr. Mater.* **2007**, *56*, 397–400. [CrossRef]
34. Chang, C.I.; Du, X.H.; Huang, J.C. Achieving ultrafine grain size in Mg–Al–Zn alloy by friction stir processing. *Scr. Mater.* **2007**, *57*, 209–212. [CrossRef]
35. Lee, C.J.; Huang, J.C.; Du, X.H. Using multiple FSP passes to cure onion splitting of Mg alloys deformed at elevated temperatures. *Mater. Trans.* **2007**, *48*, 780–786. [CrossRef]
36. Xiao, B.L.; Yang, Q.; Yang, J.; Wang, W.G.; Xie, G.M.; Ma, Z.Y. Enhanced mechanical properties of Mg–Gd–Y–Zr casting via friction stir processing. *J. Alloys Compd.* **2011**, *509*, 2879–2884. [CrossRef]
37. Yang, J.; Xiao, B.L.; Wang, D.; Ma, Z.Y. Effects of heat input on tensile properties and fracture behavior of friction stir welded Mg–3Al–1Zn alloy. *Mater. Sci. Eng. A* **2010**, *527*, 708–714. [CrossRef]
38. Padmanaban, G.; Balasubramanian, V.; Sarin Sundar, J.K. Influences of welding processes on microstructure, hardness, and tensile properties of AZ31B magnesium alloy. *J. Mater. Eng. Perform.* **2009**, *19*, 155–165. [CrossRef]
39. Commin, L.; Dumont, M.; Masse, J.E.; Barrallier, L. Friction stir welding of AZ31 magnesium alloy rolled sheets: Influence of processing parameters. *Acta Mater.* **2009**, *57*, 326–334. [CrossRef]
40. Feng, A.H.; Ma, Z.Y. Microstructural evolution of cast Mg–Al–Zn during friction stir processing and subsequent aging. *Acta Mater.* **2009**, *57*, 4248–4260. [CrossRef]
41. Xin, R.; Zheng, X.; Liu, Z.; Liu, D.; Qiu, R.; Li, Z.; Liu, Q. Microstructure and texture evolution of an Mg–Gd–Y–Nd–Zr alloy during friction stir processing. *J. Alloys Compd.* **2016**, *659*, 51–59. [CrossRef]
42. Liu, D.; Xin, R.; Zhao, L.; Hu, Y.; Zhang, J. Evaluation of corrosion and wear resistance of friction stir welded ZK60 alloy. *Sci. Technol. Weld. Join.* **2017**, *22*, 601–609. [CrossRef]
43. Liu, D.; Xin, R.; Zheng, X.; Zhou, Z.; Liu, Q. Microstructure and mechanical properties of friction stir welded dissimilar Mg alloys of ZK60–AZ31. *Mater. Sci. Eng. A* **2013**, *561*, 419–426. [CrossRef]
44. Xie, G.M.; Ma, Z.Y.; Geng, L. Effect of Y addition on microstructure and mechanical properties of friction stir welded ZK60 alloy. *J. Mater. Sci. Technol.* **2009**, *25*, 351–355.
45. Yu, L.; Nakata, K.; Liao, J. Microstructural modification and mechanical property improvement in friction stir zone of thixo-molded AE42 Mg alloy. *J. Alloys Compd.* **2009**, *480*, 340–346. [CrossRef]
46. Shen, J.; Min, D.; Wang, D. Effects of heating process on the microstructures and tensile properties of friction stir spot welded AZ31 magnesium alloy plates. *Mater. Des.* **2011**, *32*, 5033–5037. [CrossRef]
47. Chowdhury, S.M.; Chen, D.L.; Bhole, S.D.; Cao, X.; Powidajko, E.; Weckman, D.C.; Zhou, Y. Tensile properties and strain-hardening behavior of double-sided arc welded and friction stir welded AZ31B magnesium alloy. *Mater. Sci. Eng. A* **2010**, *527*, 2951–2961. [CrossRef]
48. Xu, N.; Song, Q.; Jiang, Y.; Bao, Y.; Fujii, H. Large load friction stir welding of Mg–6Al–0.4Mn–2Ca magnesium alloy. *Mater. Sci. Technol.* **2018**, *34*, 1118–1130. [CrossRef]
49. Ugender, S. Influence of tool pin profile and rotational speed on the formation of friction stir welding zone in AZ31 magnesium alloy. *J. Magnes. Alloy.* **2018**, *6*, 205–213. [CrossRef]
50. Singh, K.; Singh, G.; Singh, H. Investigation of microstructure and mechanical properties of friction stir welded AZ61 magnesium alloy joint. *J. Magnes. Alloy.* **2018**, *6*, 292–298. [CrossRef]
51. Myśliwiec, P.; Śliwa, R. Friction stir welding of thin sheets of magnesium alloy AZ31B. *Arch. Metall. Mater.* **2018**, *63*, 45–54. [CrossRef]

52. Magamai Radj, B.; Senthivelan, T. Analysis of mechanical properties on friction stir welded magnesium alloy by applying taguchi grey based approach. *Mater. Today Proc.* **2018**, *5*, 8025–8032. [CrossRef]
53. Chen, X.; Dai, Q.; Li, X.; Lu, Y.; Zhang, Y. Microstructure and tensile properties of friction stir processed Mg–Sn–Zn alloy. *Materials* **2018**, *11*, 645. [CrossRef] [PubMed]
54. Sun, S.-J.; Kim, J.-S.; Lee, W.G.; Lim, J.-Y.; Go, Y.; Kim, Y.M. Influence of friction stir welding on mechanical properties of butt joints of AZ61 magnesium alloy. *Adv. Mater. Sci. Eng.* **2017**, *2017*, 7381403. [CrossRef]
55. Singarapu, U.; Adepu, K.; Arumalle, S.R. Influence of tool material and rotational speed on mechanical properties of friction stir welded AZ31B magnesium alloy. *J. Magnes. Alloy.* **2015**, *3*, 335–344. [CrossRef]
56. Sunil, B.R.; Reddy, G.P.; Mounika, A.S.; Sree, P.N.; Pinneswari, P.R.; Ambica, I.; Babu, R.A.; Amarnadh, P. Joining of AZ31 and AZ91 Mg alloys by friction stir welding. *J. Magnes. Alloy.* **2015**, *3*, 330–334. [CrossRef]
57. Chen, J.; Ueji, R.; Fujii, H. Double-sided friction-stir welding of magnesium alloy with concave–convex tools for texture control. *Mater. Des.* **2015**, *76*, 181–189. [CrossRef]
58. Cao, X.; Jahazi, M. Effect of welding speed on the quality of friction stir welded butt joints of a magnesium alloy. *Mater. Des.* **2009**, *30*, 2033–2042. [CrossRef]
59. Pareek, M.; Polar, A.; Rumiche, F.; Indacochea, J.E. Metallurgical evaluation of AZ31B-H24 magnesium alloy friction stir welds. *J. Mater. Eng. Perform.* **2007**, *16*, 655–662. [CrossRef]
60. Lee, W.B.; Yeon, Y.M.; Jung, S.B. Joint properties of friction stir welded AZ31B– H24 magnesium alloy. *Mater. Sci. Technol.* **2003**, *19*, 785–790. [CrossRef]
61. Lim, S.; Kim, S.; Lee, C.-G.; Yim, C.D.; Kim, S.J. Tensile behavior of friction-stir-welded AZ31-H24 Mg alloy. *Metall. Mater. Trans. A* **2005**, *36*, 1609–1612. [CrossRef]
62. Chang, W.S.; Kim, H.J.; Noh, J.S.; Bang, H.S. The evaluation of weldability for AZ31B-H24 and AZ91C-F Mg alloys in friction stir welding. *Key Eng. Mater.* **2006**, *321–323*, 1723–1728. [CrossRef]
63. Afrin, N.; Chen, D.L.; Cao, X.; Jahazi, M. Strain hardening behavior of a friction stir welded magnesium alloy. *Scr. Mater.* **2007**, *57*, 1004–1007. [CrossRef]
64. Afrin, N.; Chen, D.L.; Cao, X.; Jahazi, M. Microstructure and tensile properties of friction stir welded AZ31B magnesium alloy. *Mater. Sci. Eng. A* **2008**, *472*, 179–186. [CrossRef]
65. Aydin, M.; Bulut, R. The weldability of AZ31 magnesium alloy by friction stir welding. *Kovove Mater.* **2010**, *48*, 97–103. [CrossRef]
66. Wang, X.; Wang, K. Microstructure and properties of friction stir butt-welded AZ31 magnesium alloy. *Mater. Sci. Eng. A* **2006**, *431*, 114–117. [CrossRef]
67. Yang, J.; Ni, D.R.; Wang, D.; Xiao, B.L.; Ma, Z.Y. Strain-controlled low-cycle fatigue behavior of friction stir-welded AZ31 magnesium alloy. *Metall. Mater. Trans. A* **2014**, *45*, 2101–2115. [CrossRef]
68. Motalleb-nejad, P.; Saeid, T.; Heidarzadeh, A.; Darzi, K.; Ashjari, M. Effect of tool pin profile on microstructure and mechanical properties of friction stir welded AZ31B magnesium alloy. *Mater. Des.* **2014**, *59*, 221–226. [CrossRef]
69. Chen, J.; Fujii, H.; Sun, Y.; Morisada, Y.; Ueji, R. Fine grained Mg–3Al–1Zn alloy with randomized texture in the double-sided friction stir welded joints. *Mater. Sci. Eng. A* **2013**, *580*, 83–91. [CrossRef]
70. Yu, S.R.; Chen, X.J. Microstructures and properties of FSW joints of AZ31B Mg alloy. *Adv. Mater. Res.* **2011**, *291–294*, 855–859. [CrossRef]
71. Padmanaban, G.; Balasubramanian, V. Selection of FSW tool pin profile, shoulder diameter and material for joining AZ31B magnesium alloy—An experimental approach. *Mater. Des.* **2009**, *30*, 2647–2656. [CrossRef]
72. Padmanaban, G.; Balasubramanian, V. An experimental investigation on friction stir welding of AZ31B magnesium alloy. *Int. J. Adv. Manuf. Technol.* **2009**, *49*, 111–121. [CrossRef]
73. Woo, W.; Choo, H.; Brown, D.W.; Liaw, P.K.; Feng, Z. Texture variation and its influence on the tensile behavior of a friction-stir processed magnesium alloy. *Scr. Mater.* **2006**, *54*, 1859–1864. [CrossRef]
74. Park, S.H.C.; Sato, Y.S.; Kokawa, H. Effect of micro-texture on fracture location in friction stir weld of Mg alloy AZ61 during tensile test. *Scr. Mater.* **2003**, *49*, 161–166. [CrossRef]
75. Razal, R.A.; Manisekar, K.; Balasubramanian, V. Effect of axial force on microstructure and tensile properties of friction stir welded AZ61A magnesium alloy. *Trans. Nonferrous Met. Soc. China* **2011**, *21*, 974–984. [CrossRef]
76. Esparza, J.A.; Davis, W.C.; Trillo, E.A.; Murr, L.E. Microstructure-property studies in friction-stir welded, thixomolded magnesium alloy AM60. *J. Mater. Sci.* **2003**, *38*, 941–952. [CrossRef]

77. Harikrishna, K.L.; Dilip, J.J.S.; Choudary, K.R.; Rao, V.V.S.; Rao, S.R.K.; Ram, G.D.J.; Sridhar, N.; Reddy, G.M. Friction stir welding of magnesium alloy ZM21. *Trans. Indian Inst. Met.* **2010**, *63*, 807–811. [CrossRef]
78. Xie, G.M.; Ma, Z.Y.; Geng, L. Effect of microstructural evolution on mechanical properties of friction stir welded ZK60 alloy. *Mater. Sci. Eng. A* **2008**, *486*, 49–55. [CrossRef]
79. Xie, G.M.; Ma, Z.Y.; Geng, L.; Chen, R.S. Microstructural evolution and mechanical properties of friction stir welded Mg–Zn–Y–Zr alloy. *Mater. Sci. Eng. A* **2007**, *471*, 63–68. [CrossRef]
80. Park, S.H.C.; Sato, Y.S.; Kokawa, H. Microstructural evolution and its effect on Hall-Petch relationship in friction stir welding of thixomolded Mg alloy AZ91D. *J. Mater. Sci.* **2003**, *38*, 4379–4383. [CrossRef]
81. Lee, W.-B.; Kim, J.-W.; Yeon, Y.-M.; Jung, S.-B. The joint characteristics of friction stir welded AZ91D magnesium alloy. *Mater. Trans.* **2003**, *44*, 917–923. [CrossRef]
82. Xin, R.; Li, B.; Liao, A.; Zhou, Z.; Liu, Q. Correlation between texture variation and transverse tensile behavior of friction-stir-processed AZ31 Mg alloy. *Metall. Mater. Trans. A* **2012**, *43*, 2500–2508. [CrossRef]
83. Liu, D.; Xin, R.; Sun, L.; Zhou, Z.; Liu, Q. Influence of sampling design on tensile properties and fracture behavior of friction stir welded magnesium alloys. *Mater. Sci. Eng. A* **2013**, *576*, 207–216. [CrossRef]
84. Xin, R.; Liu, D.; Li, B.; Sun, L.; Zhou, Z.; Liu, Q. Mechanisms of fracture and inhomogeneous deformation on transverse tensile test of friction-stir-processed AZ31 Mg alloy. *Mater. Sci. Eng. A* **2013**, *565*, 333–341. [CrossRef]
85. Liu, Z.; Xin, R.; Liu, D.; Shu, X.; Liu, Q. Textural variation in triple junction region of friction stir welded Mg alloys and its influence on twinning and fracture. *Mater. Sci. Eng. A* **2016**, *658*, 185–191. [CrossRef]
86. Mohan, A.; Yuan, W.; Mishra, R.S. High strain rate superplasticity in friction stir processed ultrafine grained Mg–Al–Zn alloys. *Mater. Sci. Eng. A* **2013**, *562*, 69–76. [CrossRef]
87. Prangnell, P.B.; Heason, C.P. Grain structure formation during friction stir welding observed by the 'stop action technique'. *Acta Mater.* **2005**, *53*, 3179–3192. [CrossRef]
88. Chowdhury, S.H.; Chen, D.L.; Bhole, S.D.; Cao, X.; Wanjara, P. Friction stir welded AZ31 magnesium alloy: Microstructure, texture, and tensile properties. *Metall. Mater. Trans. A* **2012**, *44*, 323–336. [CrossRef]
89. Steuwer, A.; Dumont, M.; Altenkirch, J.; Birosca, S.; Deschamps, A.; Prangnell, P.B.; Withers, P.J. A combined approach to microstructure mapping of an Al–Li AA2199 friction stir weld. *Acta Mater.* **2011**, *59*, 3002–3011. [CrossRef]
90. Xu, S.; Deng, X. A study of texture patterns in friction stir welds. *Acta Mater.* **2008**, *56*, 1326–1341. [CrossRef]
91. Schneider, J.A.; Nunes, A.C., Jr. Characterization of plastic flow and resulting microtextures in a friction stir weld. *Metall. Mater. Trans. B* **2004**, *35*, 777–783. [CrossRef]
92. Xin, R.L.; Li, B.; Liu, Q. Microstructure and texture evolution during friction stir processing of AZ31 Mg alloy. *Mater. Sci. Forum* **2010**, *654–656*, 1195–1200. [CrossRef]
93. Park, S.H.C.; Sato, Y.S.; Kokawa, H. Basal plane texture and flow pattern in friction stir weld of a magnesium alloy. *Metall. Mater. Trans. A* **2003**, *34*, 987–994. [CrossRef]
94. Bhargava, G.; Yuan, W.; Webb, S.S.; Mishra, R.S. Influence of texture on mechanical behavior of friction-stir-processed magnesium alloy. *Metall. Mater. Trans. A* **2009**, *41*, 13–17. [CrossRef]
95. Song, B.; Xin, R.; Chen, G.; Zhang, X.; Liu, Q. Improving tensile and compressive properties of magnesium alloy plates by pre-cold rolling. *Scr. Mater.* **2012**, *66*, 1061–1064. [CrossRef]
96. Barnett, M.R. Twinning and the ductility of magnesium alloys. *Mater. Sci. Eng. A* **2007**, *464*, 8–16. [CrossRef]
97. Liu, D.; Xin, R.; Xiao, Y.; Zhou, Z.; Liu, Q. Strain localization in friction stir welded magnesium alloy during tension and compression deformation. *Mater. Sci. Eng. A* **2014**, *609*, 88–91. [CrossRef]
98. Liu, D.; Xin, R.; Zhao, L.; Hu, Y. Effect of textural variation and twinning activity on fracture behavior of friction stir welded AZ31 Mg alloy in bending tests. *J. Alloys Compd.* **2017**, *693*, 808–815. [CrossRef]
99. Jonas, J.J.; Mu, S.; Al-Samman, T.; Gottstein, G.; Jiang, L.; Martin, Ė. The role of strain accommodation during the variant selection of primary twins in magnesium. *Acta Mater.* **2011**, *59*, 2046–2056. [CrossRef]
100. Lee, C.J.; Huang, J.C.; Du, X.H. Improvement of yield stress of friction-stirred Mg–Al–Zn alloys by subsequent compression. *Scr. Mater.* **2007**, *56*, 875–878. [CrossRef]
101. Xin, R.; Liu, D.; Xu, Z.; Li, B.; Liu, Q. Changes in texture and microstructure of friction stir welded Mg alloy during post-rolling and their effects on mechanical properties. *Mater. Sci. Eng. A* **2013**, *582*, 178–187. [CrossRef]

102. Xin, R.; Liu, D.; Shu, X.; Li, B.; Yang, X.; Liu, Q. Influence of welding parameter on texture distribution and plastic deformation behavior of as-rolled AZ31 Mg alloys. *J. Alloys Compd.* **2016**, *670*, 64–71. [CrossRef]
103. Yu, Z.; Choo, H.; Feng, Z.; Vogel, S.C. Influence of thermo-mechanical parameters on texture and tensile behavior of friction stir processed Mg alloy. *Scr. Mater.* **2010**, *63*, 1112–1115. [CrossRef]